Sensing and Bio-Sensing Research 7 (2016) 62–70

Contents lists available at ScienceDirect

Sensing and Bio-Sensing Research

journal homepage: www.elsevier.com/locate/sbsr

Propagating and localized surface plasmon resonance sensing — A critical comparison based on measurements and theory

Jacqueline Jatschka, André Dathe, Andrea Csáki, Wolfgang Fritzsche, Ondrej Stranik *

Nanobiophotonic Group, Leibniz Institute of Photonic Technology, Jena, Germany

ARTICLE INFO

Article history:
Received 5 October 2015
Received in revised form 2 January 2016
Accepted 8 January 2016

Keywords:
Plasmon
Sensing
Nanoparticles
Metallic layers
Spectroscopy
thin-layer adsorption

ABSTRACT

With its potential for ultrasensitive, label-free detection of molecular interactions, sensing methods based on the surface plasmon resonance (SPR) effect fully meet the requirements for modern analytical techniques. Already established by using propagating SPR in thin gold layers, the last years witnessed the emergence of another related technique utilizing extremely miniaturized noble metal sensor structures, based on a localized SPR.
This paper provides a critical comparison of these kinds of SPR sensing, reviews the foundation of both general approaches, presents experimental data on exactly the same molecular model system using both techniques, as well as theoretical considerations in order to allow reasonable comparison. It highlights the specific features and effects, in order to provide guidance in choosing the right technique for given bioanalytical tasks.
The study demonstrated the capabilities of LSPR for sensing of molecular layers even in the lower nanometer dimension. For the detection of small (bio)molecules, smaller particle diameters are favored regarding highest sensitivity. It also presents an approach to obtain refractive index and the thickness of a molecular film by analyzing the signal response of plasmonic sensors with metal nanoparticles. Moreover, an additional method for the improvement of the parameters' determination is introduced.

1. Introduction

Detection of biomolecular binding, the adsorption of thin bio-films or conformational changes of macromolecules is of high interest in various branches of biology, medicine and pharmacy [1]. One possible detection method is based on the optical spectroscopy of metallic structures exhibiting surface plasmon resonances [2]. It represents a label-free approach, with rather high sensitivity in comparison to other label-free techniques. In this detection scheme, the molecular binding occurs near the surface of the metallic structures, in which the light is captured in the form of surface plasmon polaritons. The excitation of the surface plasmon polaritons requires specific illumination conditions such as illumination wavelengths and incident angles. These excitations are also strongly sensitive on the presence of the molecules on the surface, and therefore, the changes in the plasmon excitation indicate molecular adsorption events. The established method of such sensing (a wide range of commercial products is available on the market [3,4]) is by using thin smooth metallic layers [5,6] (propagating surface plasmon resonance — pSPR), which achieve remarkably low limits of detection. However, this basic geometry of the metallic structure does reach its maximal sensitivity for very small molecules (few nanometers), because the spatial confinement of the plasmon modes (~several hundred nm) is still much larger than these molecules (~few nm) and complex immobilization strategies using thick hydrogels are used to compensate the spatial mismatch. Avoiding the critical surface chemistry, this could be also overcome by either structuring the smooth layers or by using more spatially confined nanostructures (exhibiting localized surface plasmon resonances — lSPR) instead of metallic layers [7–12].

The first objective of our work was to compare the signal responses from plasmonic sensors with different geometries (implicating different spatial confinement of the generated plasmons). The second objective was to compare signal responses from sensors with different numbers of nanostructures (ensemble versus single nanostructure). In order to make the comparison, for both measurements the same model system is used, namely the sequential adsorption of thin polymer layers of defined thickness and number (also known as layer-by-layer technique). Additionally, we were interested if both thickness and refractive index of the adsorbed layer can be obtained by adjusting the volume of the plasmon.

The results of these direct comparisons reveal the advantages and disadvantages of each plasmonic transducer and their best applicability. The information about thickness and refractive index of the adsorb layer would be quite useful, because it can be used to determine the density of the adsorbed layers. Thereby, for example, conformational changes of molecules in the layer could be monitored. Unfortunately, the established plasmonic sensing using gold films yields only the average mass adsorbed on the surface. However, as shown by Hull

* Corresponding author.
E-mail address: ondrej.stranik@ipht-jena.de (O. Stranik).

http://dx.doi.org/10.1016/j.sbsr.2016.01.003

[13], the conformational changes of proteins can be deduced if there is enough spatial confinement of the plasmon.

In the article we compare plasmonic transducers with different spatial confinement: a planar gold layer, and spherical gold nanoparticles of different sizes. We analyzed the responses of these systems and experimentally measured their responses to the subsequent adsorption of molecular layers. We showed that the nanoparticles with a short plasmon confinement yield a non-linear dependence of the signal on the number of deposited layers. By analyzing the non-linear response of the signal, the refractive index and the thickness layer can be obtained in principle. We experimentally demonstrate that adsorption of individual layers can be detected even on a single nanoparticle and discuss the method of obtaining refractive index and thickness of the layer adsorbed on single nanoparticle (NP) level.

Briefly, we present the reader experimental data demonstrating the effect of spatial confinement of the plasmon on the signal response with identical adsorption layers and show the determination of the layer thickness and refractive index of these layers by analyzing the non-linear signal response.

2. Background

2.1. Geometry of pSPR and lSPR detection

In the following section the detection principles on thin metallic layers and metallic spherical nanoparticles are recalled and an effective refractive index is defined in order to compare the signals from the pSPR and lSPR systems. Standardly, the plasmon waves in a thin metallic layer are excited by the illumination of the metallic films on its back side attached to a prism with a high refractive index (Kretschmann configuration see Fig. 1). If the condition of momentum conservation for the illumination light and the plasmon (angle of incidence) and the condition of the energy conservation (wavelength of the incident light) are fulfilled, the light is coupled to the plasmon waves (with evanescent field on the top side of the films), and the coupling leads to an intensity drop in the reflected light [14]. The pSPR instrument used in the experiments utilized a monochromatic light with a range of incident angles. Therefore, the plasmon excitation corresponds to the minimum in the graph of the reflectivity on the incident angle (see Fig. 1). Upon the change of refractive index in the vicinity of the layer, the coupling condition changes and the peak's minimum shifts. On the other hand, the localized plasmons in metal nanoparticles are excited by direct illumination independently of the angle. If the condition on energy (wavelength of the incident light) is fulfilled than the light is coupled to the plasmon (with an evanescent field around the NP) and leads to intensity drop in the transmitted light [15]. Therefore, the plasmon excitation corresponds to the maximum observed in absorbance (see Fig. 1 — right side down). Upon changes of the refractive index in the vicinity of the NPs, the coupling condition changes and leads to a shift of the peak maximum.

2.2. Signal analysis from SPR and LSPR system

The electric field of plasmons excited on a thin metallic layer (pSPR) is analytically described by an exponential function [14] (Table 1, Eq. (1a)). The associated E-field is maximal at the interface and it decays exponentially into the dielectric bulk material. The rate of the decay is given by the parameter penetration depth (L_{pd}), which depends only on optical properties of both metal and bulk at a given wavelength. Although the E-field can be theoretically compressed to volumes much smaller below the diffraction limit, in real metals the compression is still much larger then sizes of typical biomolecules (~few nanometers). In our setup the theoretical value of L_{pd} was 318 nm. Also in case of a plasmon generated on a spherical nanoparticle (lSPR), the associated E-field is maximal at the surface of the particles and then steeply decays into the dielectric bulk. In the electrostatic approximation, the profile can be described by a simple analytical expression, where the decay depends on the order of the mode and the radius of the particle [16] (Table 1, Eq. (1b)). For 20 nm diameter gold nanoparticles for example, the E-field of dipole modes ($p = 1$) drops at approx. 3 nm down to the half. Therefore, the localized plasmon can be much stronger spatially confined then propagating plasmons, and this confinement is determined by the nanoparticle size. The electric fields' profiles (calculated with full electromagnetic theory) of propagating and localized plasmon on nanoparticles with different radius are displayed in Fig. 2 (right).

In order to compare the performances, the same signal has to be defined for both systems, what can be done in the following way: The

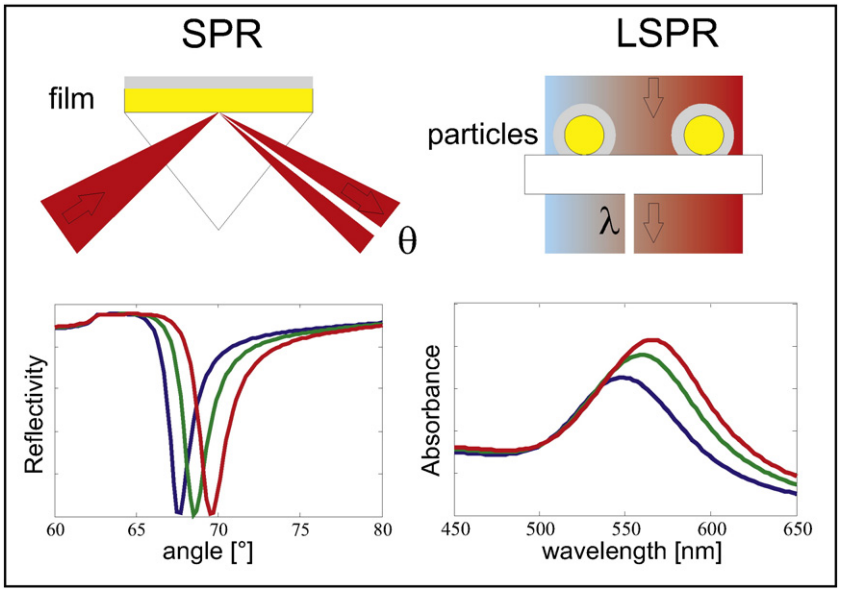

Fig. 1. Schematics of the sensing principle for the studied pSPR (left) and lSPR (right) systems. The graphs below show the calculated shift of dip/peak upon adsorption of 10 nm (green line) and 20 nm (red line) thick molecular film with an refractive index of 1.48 in water ($n = 1.33$), which mimics the properties of biomolecules.

Table 1
Comparison table with equations describing the electric fields, the comparable instruments signal and signal change upon adsorption of molecular layers for propagating and localized surface plasmon, respectively. The following symbols were used in eq (1): L_{pd} — penetration depth, h — distance from metal surface, n_m — metal refractive index, n_b — bulk refractive index, λ — illumination wavelength, r — radius of the nanoparticle, p — order of the plasmon mode. Eq. (2), n_l — refractive index of layer, θ_{res} — plasmon resonance angle, λ_{res} — plasmon resonance wavelength, S_b^p, S_b^l — bulk sensitivity (propagating, localized). Eq. (3) d — thickness of adsorbed layer.

Equations of	(a) pSPR	(b) lSPR	
E-field profile	$\lvert E(h)\rvert = E_{,max} * \exp(-\frac{h}{L_{pd}})$ $L_{pd} = \lambda/Re\{2\pi i * \frac{n_m^2}{\sqrt{n_m^2+n_b^2}}\}$	$\lvert E_p(h)\rvert = E_{,max,l} * (1+\frac{h}{r})^{-(p+2)}$	(1)
Instrument's signal	$\Delta n_{eff}(d, n_l, n_b) \equiv \frac{\Delta\theta_{res}}{S_b^p}[RIU]$	$\Delta n_{eff}(d, n_l, n_b) \equiv \frac{\Delta\lambda_{res}}{S_b^l}[RIU]$	(2)
Adsorption of a thin layer	$\Delta n_{eff} = (n_l - n_b)d\ \frac{2}{L_{pd}}$	$\Delta n_{eff} = (n_l - n_b) * (1-(1+\frac{d}{r})^{-(2p+1)})$	(3)
Signal enhancement	$S_{enh} = \frac{\Delta n_{eff}\lvert lSPR}{\Delta n_{eff}\lvert pSPR} = \frac{2p+1}{2}\frac{L_{pd}}{r}$		(4)

change of the bulk refractive index around the plasmonic structures induces the shift of the dips and peaks in the signal of pSPR and lSPR, respectively. One defines the parameters bulk sensitivity S_b^p, S_b^l as the measure of the dip shift and peak shift on the change of the bulk refractive index for pSPR and lSPR systems, respectively. If the variation in the bulk refractive index is relatively small, S_b^p and S_b^l will have constant values and these can be experimentally determined. Using these bulk sensitivity values, a comparable signal - change of effective refractive index (Δn_{eff}) — measured in RIU units for pSPR and lSPR can be defined (Table 1, Eq. 2ab).

Following this signal definition, for a change of the bulk medium, Δn_{eff} is equal to the difference of the refractive index of the mediums. If a thin layer is adsorbed on the surface, then Δn_{eff} depends not only on its refractive index, but also on the layer thickness and the E-field extension from the surface. Analytical expressions of Δn_{eff} for pSPR and lSPR can be derived (see supplementary information) and their formulas are displayed in Table 1, Eq. 3ab, which give qualitative insight into the Δn_{eff} dependence on a thin layer adsorption. These expressions are identical with the more rigorous analysis done in [17] (for the case of pSPR) and in [18] (for lSPR with p = 1). In pSPR sensing, the E-field changes slowly throughout the organic layer, and so Δn_{eff} is directly proportional to the product of the thickness and refractive index of the layer. In our experimental measurements, L_{pd} is ~300 nm, which is much larger than investigated layers. On the other hand, the E-field in the case of LSPR sensing is decaying much quicker (radius of the nanoparticle ~tens of nanometers), and therefore, Δn_{eff} has a non-linear dependence on the thickness of the layer. By dividing Eq. 3b through 3a in Table 1 and using the Tailor expansion for very thin layers ($d \ll r$), an approximate expression of the Δn_{eff} signal enhancement of lSPR over pSPR (S_{enh}) is obtained (Eq. 4, in Table 1). If the sizes of the nanoparticles are much smaller than the penetration depth of the pSPR system, a considerable signal enhancement is observed.

As an illustrative example, the dependence of Δn_{eff} on the product of the thickness and refractive index of the layer together with the E-field

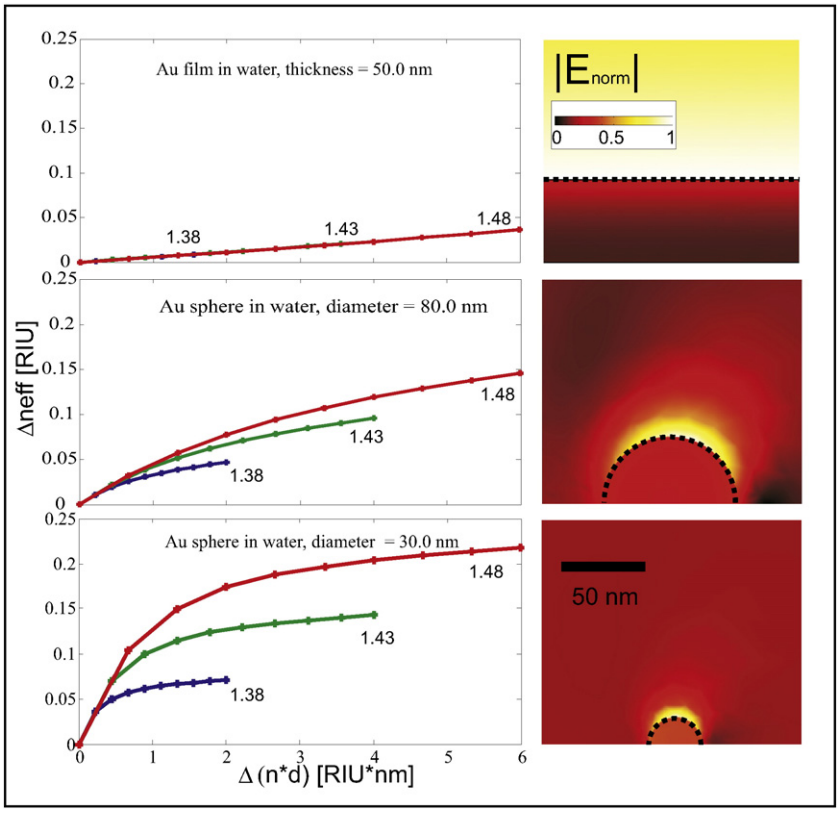

Fig. 2. Theoretically calculated dependence of the instrument signal Δn_{eff} on the product of refractive index of the layer (relative to the embedded medium, water n = 1.33) and the layer thickness. The different curves correspond to the different refractive indexes of the adsorbing layer (numbers along the curves). Top — propagating SPR on a gold layer, Middle —localized SPR on a gold sphere (radius 40 nm), Bottom —localized SPR on a gold sphere (radius 15 nm). Left images — absolute values of electrical field normalized on its maximal value around each nanostructure in the plasmon resonance. The strong spatial field localisation for lSPR system is clearly visible.

profile around the nanostructure for pSPR and lSPR systems are plotted in Fig. 2. These graphs and E-field distributions were calculated with exact solutions of Maxwell equations for stratified medium and Mie theory of pSPR and lSPR, respectively. From the E-field images one can nicely see that the E-field of the pSPR extends much more than the lSPR field, and that the decay of the E-field in lSPR is influenced by the radius of the nanoparticle. The graphs of Δn_{eff} confirm the linear and non-linear dependence on the thickness for pSPR and lSPR, respectively, and that the non-linear dependence of the layer thickness can be tuned by the radius of the nanoparticle.

The graph in Fig. 2 (together with Eq. 3a in Table 1) also illustrates that it is not possible to detect conformational changes by pSPR systems. The product of the thickness and refractive index of the layer ($n * d$) depends only on the surface density of the adsorbed molecules because the change of the refractive index is compensated by the inverse change of the thickness [19]. Therefore, Δn_{eff} in pSPR system does not change if the refractive index and the thickness of the layer are modified by conformational changes of the molecules. This is illustrated by the identical curves in Fig. 2 (top graph). However, the strong E-field confinement in lSPR system allows detecting these conformational changes. The curves in Fig. 2 (middle, bottom graphs) show that with $n * d$ keeping constant but modifying the refractive index, the signal is changed. These properties of the Δn_{eff} will be later used for obtaining parameters of thin layers.

3. Materials and methods

3.1. Preparation of chips for LSPR sensing

Glass slides were cleaned by hand with rinsing agent and further with acetone, ethanol and water in ultrasonic bath for 10 min each. Afterwards the glass slides were cleaned by oxygen plasma etching for 1 h at 380 W. The affinity of the gold nanoparticles to the surface was increased by functionalizing the glass slides with an amine surface group. Therefore, the chips were incubated with 1% APTES (*3-aminopropyltriethoxysilane*) (Carl Roth GmbH & Co. KG, Germany) in 1 mM acetic acid for 10 min, followed by washing with water in an ultrasonic bath. For the eLSPR measurements, solutions with spherical gold nanoparticles with diameters of 30 nm, 60 nm and 80 nm from British BioCell International (UK) were centrifuged with 8000 rpm for 6 min. The supernatant was removed and 20 μl of the nanoparticles solution was pipetted in the center of the glass chip. For the sLSPR measurements, the density of immobilized NPs was decreased in order to image each single NPs separately by optical microscopy. Therefore, the 80 nm gold particle stock solution was diluted 1:10 with deionized water, and this solution was pipetted on the chip, fully covering it. After an incubation time of 1 h, the glass slides for both measurements were rinsed with water and dried with nitrogen. The surface distribution of the adsorbed nanoparticles was determined by an Atomic force microscope Dimension TM 3100 with a Nanoscope IIIa controller (Digital Instruments, Veeco, USA).

3.2. Chip integration with microfluidics

The microfluidic chamber was custom-designed and consisted of a 35 × 16 mm glass slide with drilled holes, pressure sensitive adhesive layers on top and bottom sandwiched between an overhead transparency (bottom) and the chip with immobilized NPs (top). Prior the chamber assembly the glass slides were cleaned with the same procedure as the cleaning of LSPR chips. The created chamber had a height of around 100 μm and the volume was around 7 μl. The chamber was connected to a syringe pump Legato (kdScientific, USA) controlling the flow rates of the buffer together with an injection valve allowing injection of 150 μl solutions in the chamber.

3.3. Ensemble LSPR (eLSPR) measurement

The eLSPR measuring setup included a halogen light source (HL-2000-FHSA from Ocean Optics, USA), and a UV–VIS linear photodiode array spectrometer Cypher II (B&WTech, USA). The light was directed and collected on a self-made microfluidic chamber by multimode optical fibers. Prior to the measurement, spectra of dark current and the lamp were recorded. The online detection was controlled by a custom built LabView program and the data analysis was carried out with homemade Matlab software. In order to minimize the noise of position of the LSPR peak, the centroid of the LSPR peak was calculated as in [20].

3.4. Single particle lSPR measurement

Nanoparticles immobilized in the microfluidic chamber were observed by an optical microscope Axio Imager Z1m (Carl Zeiss Micro-imaging, Göttingen, Germany) in dark-field mode similar as in [21]. The illumination source was a tungsten halogen lamp having a continuous broad band spectrum. The scattered light from a single nanoparticle was collected via a multimode fiber with a pinhole of 100 μm placed at the image plane of the microscope. The fiber was connected to an Acton Research SpectraPro 2300i micro spectrometer (Princeton Instruments, Trenton, NY) with a grating of 150 lines per mm and a peltier-cooled CCD camera Pixies 256 (Princeton Instruments, Trenton, NY). In order to minimize the noise in LSPR peak position, the centroid of the LSPR peak was calculated as in [20].

3.5. SPR measurement

SPR measurements were realized with a dual channel SPR Instrument Reichert SR7000DC (Reichert Inc., Depew, USA) connected to a syringe pump. As substrates, 12.5 × 12.5 mm gold coated glass slides (0.33 mm glass slide, a 10 Å chromium layer and a 500 Å gold layer) from XanTec bioanalytics GmbH (Düsseldorf Germany) were used. The illumination wavelength was 780 nm. The SPR chips were cleaned by oxygen plasma etching for 10 s at 380 W.

3.6. Bulk sensitivity calibration

A refractive index calibration solutions series was prepared by aqueous glucose solutions of concentrations ranging from 0 to 30% by weight. Their refractive index was measured by a refractometer PAL-RI (Atago, Tokyo, Japan). These glucose solutions were injected into the detection system with the running buffer being deionized water, and the signal response was recorded.

3.7. Molecular layers deposition protocol

Molecular layer deposition was based on self-assembly of alternatively charged polymers from solution [22]. Polyelectrolyte solutions were prepared as following: 1 mg/ml anionic poly(allylamine hydrochloride) (Mw ~ 58,000) (PAH) and poly(sodium 4-styrenesulfonate) (Mw ~ 70,000) (PSS) were diluted in 0.5 M sodium chloride water solution, respectively. All the reagents were purchased from Sigma Aldrich (Taufkirchen, Germany). The measurement of the thin layer formation on the plasmonic transducer was done on-line during the alternating injection and flow of the polyelectrolytes (starting with PAH) in the microfluidic chamber in the case of SPR and LSPR systems. At the beginning, a running buffer of 0.5 M sodium chloride was flowing with the rate of 100 μl/min, until the signal stabilized. Afterwards, the flow rate of the buffer was reduced to approx. 20 μl/min, and 200 μl of polyelectrolyte solutions were alternately infused. In between each layer deposition, the chip was rinsed with the buffer solution.

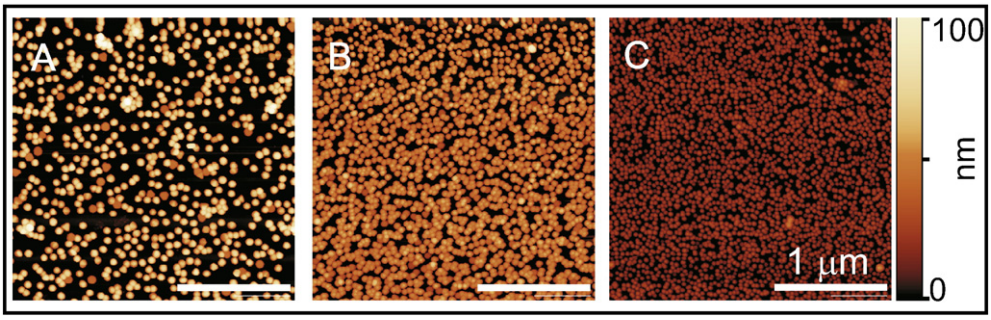

Fig. 3. Atomic force microscopy of the substrates with immobilized gold nanoparticles with radius of 40 nm (A), 30 nm (B) and 15 nm (C).

3.8. Simulation of signal response from the pSPR and lSPR system

The reflection spectra from the thin metallic layer were calculated with the exact solutions of Maxwell equations for stratified medium [23]. The extinction spectra and scattering spectra of the spherical nanoparticles with a shell were calculated with Mie Theory [15]. The peak/dip position was determined in the same manner as in the experiment (centroid position) [20]. The bulk sensitivities of the systems were determined by calculating the peak/dip shift for the refractive index from 1.33 to 1.43. The signal change Δn_{eff} for the pSPR and lSPR system was determined by calculating the peak/dip shift upon addition of the thin layer and dividing this value by the corresponding bulk refractive index. The refractive index of the gold was taken from reference [24].

4. Results and discussion

4.1. lSPR Chips characterization

Glass chips with densely immobilized NPs with three different diameters (80 nm, 60 nm and 30 nm) were prepared. Visually the chips had a uniform red color over the area (~0.25 cm^2) with the immobilized nanoparticles. AFM images from the center of the area with immobilized NPs were recorded and are presented in Fig. 3. The images show a rather homogeneous NP distribution on the surface without any significant NP aggregation. The height of the NPs is relatively uniform and the average height corresponds to the given diameters of the NPs in all three cases. It is apparent that the surface concentration of the NPs is increasing with decreasing NP size. Larger NPs have a higher total charge on their surface causing a stronger repulsion between the NPs. This leads to larger spaces between the immobilized NPs.

4.2. Measurement of bulk refractive index

These chips were incorporated into the microfluidic chamber and the optical detection system (the instrument details are presented in Figure S5 — supplementary information). Solutions with known refractive index were used to determine the bulk sensitivity S_b^l of the lSPR for different sizes of the NPs; they are summarized in Table 2. The data showing the shift of the plasmon resonance upon the bulk refractive index changes are given in Figure S1 of the supplementary information. The data show that the bulk sensitivity of the lSPR is increasing with the size of the used particles, which is in an agreement with the theory. From the peak position variation over time the lowest detectable Δn_{eff} is determined to be better than 10^{-4} RIU. The used commercial pSPR system (the instrument details are presented in Figure S5 — supplementary information) gave the lowest detectable Δn_{eff} around 10^{-6}. The Δn_{eff} signals yield in both pSPR and lSPR the same values for the bulk measurement. Again, these values show that the pSPR system is significantly better in the determination of the bulk refractive index. These values are – beside the physical principles – also influenced by the instrumentation, which is very well established in the SPR systems. Intuitively, there is no advantage of a stronger E-field confinement for the bulk measurement of refractive indexes, however its benefit is present for measurements of thin films.

4.3. Measurement of molecular layer adsorption

As a model of thin molecular layer adsorption, the well-controllable system of polyelectrolyte layers (PEL) was chosen [25]. Polyelectrolytes are charged polymers, which adsorb from a solution on a (oppositely charged) surface and form a monomolecular layer with a defined, constant thickness in the lower nm range, which can be tuned by the salt concentration in the solution. The effect is based on electrostatic adsorption, and therefore multilayers can be realized by the alternative adsorption of positively and negatively charged PEL.

Both pSPR and lSPR systems were used to study the adsorption of the PEL layers. The alternatively charged PEL solutions were flown over the substrates (gold layers or gold nanoparticles) with a washing step in between. The signal changes after the adsorption of first four layers are presented in Fig. 4 (lSPR — NP diameter = 80 nm). The curves in both systems demonstrate the adsorption of each layer as well as the self-termination of PEL adsorption.

The adsorption of up to twenty subsequent PEL layers was followed with the lSPR (for all three NP diameters: 15, 30 and 40 nm) and the pSPR system. The data are shown in Fig. 5. The dependence on the number of deposited PEL layers is linear in the case of the pSPR system, but in the case of lSPR system, it is non-linear with an asymptotic value around 0.2 RIU for all NPs types. The data also show that maximum values of Δn_{eff} are achieved quicker for the smaller NPs. These measurements results have the same tendency as the calculated example data in Fig. 2, so they confirm the changing efficiency of the E-field confinement around the different metallic structures (as explained in the previous section). Moreover, the data show that the E-field confinement leads to an increase of signal Δn_{eff} for the lPSR signal in comparison to the pSPR signal, and therefore, improves the limit of detection. The strongest

Table 2
Experimental bulk sensitivities of the different lSPR systems.

	elSPR (r = 15 nm)	elSPR (r = 30 nm)	elSPR (r = 40 nm)	pSPR on layer
S_b bulk sensitivity	49.1 nm/RIU	57.8 nm/RIU	90.0 nm/RIU	
n_{eff} precision [RIU]		$<10^{-4}$		$<10^{-6}$

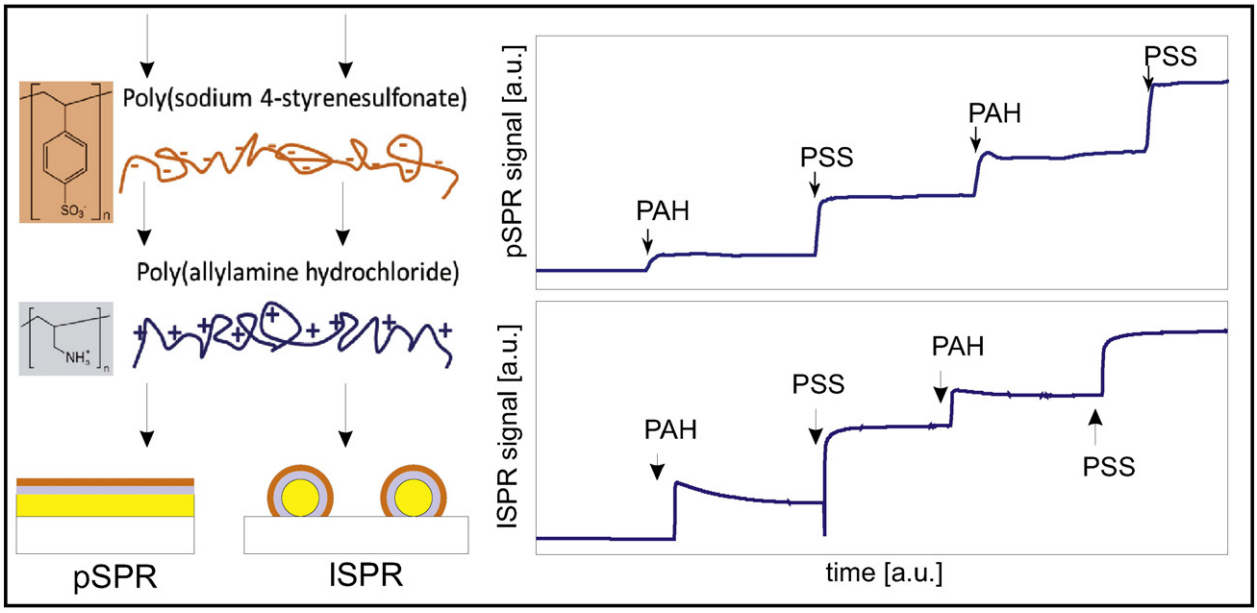

Fig. 4. Left — schematics of the adsorption on the plasmonic structures and chemical structures of the used PEL. Right — Examples of the adsorption of the first four poly-electrolyte (PEL) layers measured by pSPR and lSPR system (sphere, r = 40 nm).

signal enhancement is thereby achieved by the lSPR system for the smallest spheres (r = 15 nm) and for the first layers, where the values reach more than 40 times (2 PEL layers — Δn_{eff} (pSPR) = $2.09 \cdot 10^{-3}$ RIU, Δn_{eff} (lSPR) = $8.6 \cdot 10^{-2}$ RIU). This represents a quite useful improvement of the signal and it roughly fits to the theoretical value from Eq. 4. On the other hand, the dynamic range of the layer thickness detection is reduced. It means that special care has to be taken on a choice of the nanoparticle size depending on size of the target biomolecules, the mode of the plasmon resonance and the type of application (molecule detection or detection of molecule's conformational changes).

4.4. Single particle lSPR measurement of thin layer adsorption

The fundamental advantage of the lSPR compared to the pSPR sensing is the 3-dimensional spatial localization of the detection volume. The effect of lateral confinement is lost in the case of lSPR measurement on an ensemble of metallic nanoparticle as done in the previous experiment (ensemble lSPR are excited everywhere on the substrate). The single particle lSPR measurement can be carried out with a microspectroscopy combined with dark-field illumination set-up [21]. With the additional integration of the microfluidic system into the microscopy set-up (the instrument details are presented in Figure S5 — supplementary information), it was possible to measure the adsorption of individual PEL layers on a single 80 nm diameter gold NP. The dark field images of the NPs are displayed in Fig. 6 right. The bottom image shows the bare single NPs (green color) and the top image represents the NPs after a deposition of 12 PEL layers. The two images show that nanometer thin layer adsorption on an area of less than 0.02 um^2 (approximate size of the nanoparticles) is even detected by simple RGB-imaging only. The signal change Δn_{eff} after deposition of each PEL layer on a selected single NP (indicated by a circle in the images) is given in Fig. 6 left. For comparison, Δn_{eff} for ensemble measurement for the same NP size is also shown. Both curves confirm subsequent adsorption of the PEL layers, but the rate of the signal change is different. The differences originate from the fact that the local adsorption at the NP is not identical with the average adsorption of the PEL layer and that the measured NP geometry can deviate from the average size of the NPs. The disadvantage of the single particle lSPR is the much higher noise of the signal. The measured n_{eff} precision on bare nanoparticles was around 0.01 RIU (see the experimental data in supplementary information Figure S3), and during the PEL layer adsorption around 0.02, which is two orders of magnitude higher than in the case of the ensemble lSPR measurement. There are several reasons for the larger noise. First, in the single particle lSPR measurement, less photons are available. In single particle lSPR only the photons scattered from a single NP are detected. On the other hand, in eLSPR measurement, large number of photons reach the spectrometer, which are actually not scattered/absorbed by nanoparticles. This effect leads to worse signal-to-noise-ratio (photon fluctuation is proportional to the square root of the number of photons), a stronger background signal, longer integration time (meaning time averaging is hampered). Secondly, in the single particle lSPR, a focusing optics with high numerical aperture is used to increase the collection efficiency of the scattered photons from the area of the single particle. Nevertheless, this optical collection is very sensitive to small mechanical movement/vibrations occurring during the measurement, and thereby increases the signal noise.

4.5. Obtaining the thickness and the refractive index of layers

Generally, information about the absolute thickness of the layer of the adsorbed molecules and its refractive index can give deeper insight into the conformation state of the molecules and their density. As

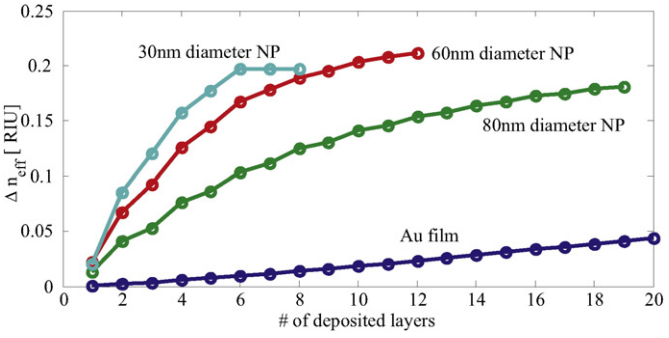

Fig. 5. Experimentally measured change of effective refractive index Δn_{eff} upon the deposition of series of molecular layer on various plasmonic sensors. (Layer corresponds to pSPR system. NP corresponds to lSPR system with nanoparticles of different diameter). The error of the Δn_{eff} determination was less than 10^{-3} RIU and it was governed by the variation in polymer adsorption kinetics.

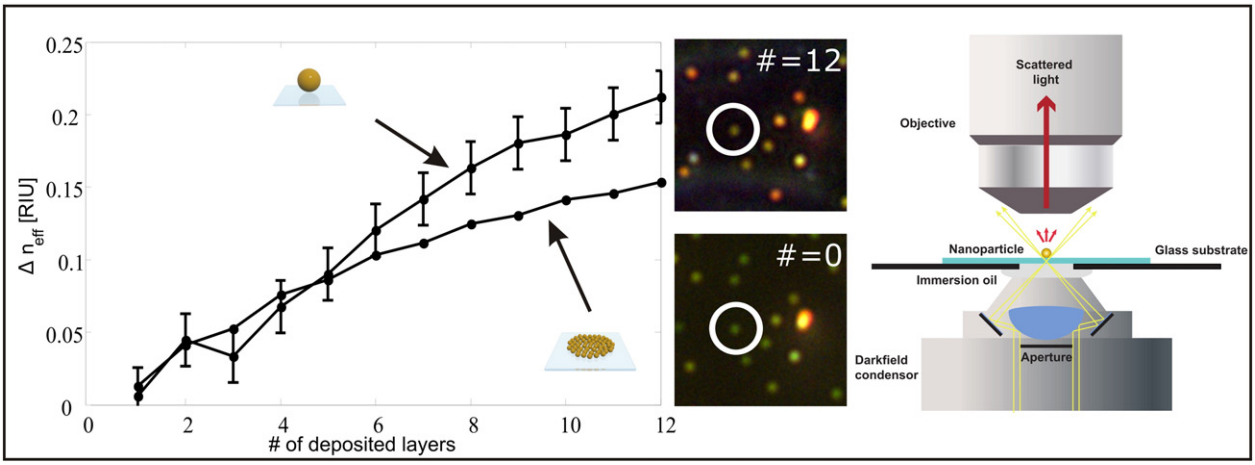

Fig. 6. LSPR measurements for 80 nm gold spheres for a single particle as well as for an ensemble. Insets: Dark-field image of the studied single particle before layer deposition (bottom) and with 12 layers (top), and scheme of the measurement setup (right).

explained earlier, the non-linear signal behavior of lSPR signal upon adsorption of thin layers (Table 1, Eq. 3b) allows in principle to determine these parameters. However, they cannot be obtained from a single measurement, because Δn_{eff} is a function of the refractive index and the thickness. In the case of PEL adsorption, if the same thickness of each adsorbed PEL layer is assumed, measurement of Δn_{eff} for several adsorbed PEL layers allows fitting of values for the refractive index and the thickness of the PEL.

The quality of the fit for three different NPs in the lSPR system is displayed in Fig. 7. The color maps show reciprocal values of the differences between the sum of the measured values of Δn_{eff} and the calculated Δn_{eff} for given refractive index (x-axis) and the average layer thickness (y-axis). The position of the maximum value in the color map yields the fitted parameters, which are summarized in the table at the bottom of Fig. 7. The measurement with the 15 nm radius NP gave smaller layer thickness and higher refractive index then the measurements with 30 nm or 40 nm radius NP. This deviation could be explained by the fact that the initially deposited layers are usually more compact [26], and the measurement with 15 nm radius NP were done on less PEL layers (8) then the other measurements (12 and 19).

Another approach for the determination of the refractive index (n) and layer thickness (d) is to obtain two signal changes Δn_{eff} by two detection systems having plasmons with different E-field confinement. This leads to two independent equations for two unknown parameters n and d. Such approach was already investigated on modified planar system either by addition of complex wave guiding layer [27] or creating special gratings [28,29]. With larger differences in the E-field confinement of the different plasmons, a better determination of the parameters is possible. Due to the good tunability of the E-field confinement by the size of the NPs, we applied this method to the determination of refractive index and thickness of PEL layer by analyzing Δn_{eff} obtained from the previous lSPR measurement.

For the analysis, the values of Δn_{eff} on 15 nm and 40 nm radius nanoparticles in lSPR measurements were used. These Δn_{eff} values were plotted against each other in the graph in Fig. 8, where each dot represents different number of PEL layers. Further, the lines for layer adsorption with the constant refractive index (from 1.34 to 1.63, steps of 0.01) and constant total thickness (from 1 to 16 nm, steps of 1 nm) in the space Δn_{eff} (40 nm radius NP) and Δn_{eff} (15 nm radius NP) were calculated (by the same method as previously) and plotted in the same graph as the experimental data in Fig. 8. The positions of the point with respect to the isolines determine the sought parameters, which are summarized in the table in Fig. 8. With this method, in contrast to the previous methods, it was now possible to obtain the total thickness and refractive index for each deposited layer. The parameters are changing with the number of the deposited layer.

Surely, the results were burden with larger experimental uncertainty (especially for the first layers), because the experimental data of the PEL adsorption were obtained for two different measurements with probably slightly variation in the adsorption. Nevertheless, the results show the possible application of this method for lSPR sensing. Utilizing a mixture of two different nanoparticles with different sizes for lSPR sensing (with sufficiently spectrally separated peak positions) can resolve this issue.

In order to determine the thickness of the adsorbed layer on a single particle level, the previously used method of having a combination of two particles cannot be used. It is necessary that two plasmon modes with different E-field confinements are generated on the same NPs. We suggest that this can be done by using larger spherical NP exhibiting not only the plasmon dipole mode, but also the quadrupole mode,

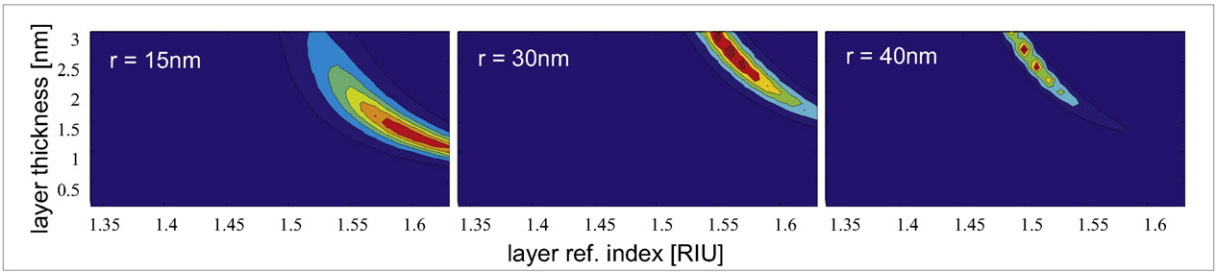

Fig. 7. Color map of the fit quality for different PEL layer thicknesses and refractive indexes in case of NPs with different radius (red — high quality of the fit, blue — low quality of the fit). Table — Fitted parameters of the PEL layers (average refractive index, thickness of single PEL layer) from measurements on 15 nm, 30 nm, 40 nm radius particles.

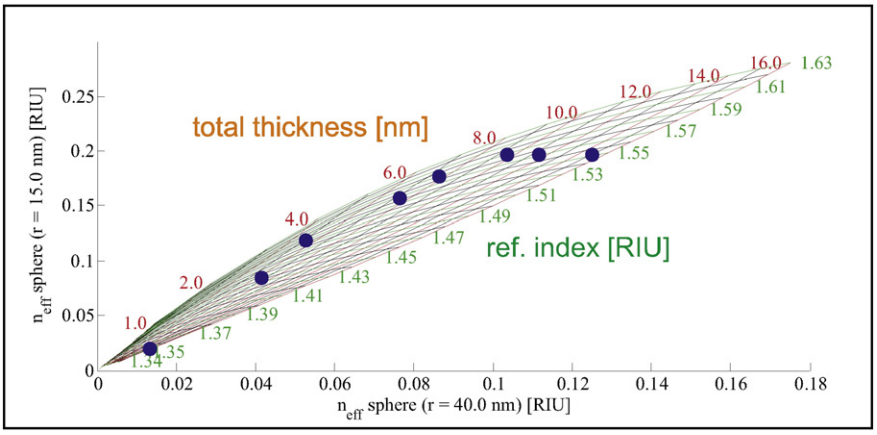

Fig. 8. A graph presenting calculated contour lines with constant refractive index (green) and constant total layer thickness in nm (red) in a space of the effective refractive index of 15 and 40 nm radius sphere, respectively. Blue dots are experimentally measured effective refractive indexes for each deposited layer. In the table below are the average refractive index and the total thickness of the layer after each subsequent layer deposition estimated from the graph.

which confines the E-field stronger then the dipole (see Eq. 1b in Table 1). The position of the quadrupole mode is at shorter wavelengths than the dipole mode. The quadrupole in the gold NPs are hard to observe, because gold is strongly absorbing at shorter wavelength (d-band electron absorption). Therefore, we suggest using larger silver spherical NPs, where the dipole and quadrupole peaks can be measured [30]. As an example, the dependence of the Δn_{eff} for dipole and quadrupole mode in case of 40 nm radius Ag NP on the adsorption of the thin layers was calculated and is plotted in Figure S4 (supporting information). The different profiles of the Δn_{eff} curves for the dipole and quadrupole indicates the possibility to obtain the thickness and the refractive index of the adsorbed layer by fitting both Δn_{eff}.

5. Conclusion

In this work, we experimentally compared the performances of various label-free sensor arrangements based on surface plasmon resonances (propagating and localized) by measuring the same system, which was prepared by well controllable, sequential deposition of charged polyelectrolyte layers. The geometries of the plasmonic transducer were the following: planar gold films (pSPR), ensemble of gold nanoparticles with three different sizes (ensemble lSPR), and single gold particle (single particle lSPR). In order to compare the systems, we defined a signal response Δn_{eff} from all the sensors. By analyzing its dependency on the adsorption of thin layers theoretically, we showed that the lSPR signal has a non-linear dependency on the number of deposited layer (opposite to the pSPR), that the signal depends on the size of the nanoparticle pSPR, and that there is a large signal change in comparison to pSPR. This analysis was in agreement with the experimentally measured data. In comparison to pSPR, the highest lSPR signal improvement was in the case of 30 nm diameter gold nanoparticle and the first adsorbed layers. Although the background noise of the signal on the pSPR signal was much lower than in the ensemble lSPR, the signal noise during the PEL deposition was governed by the variation of the adsorption process, therefore minimizing this advantage at least for the studied model system. We also showed that it is possible to detect sequential adsorption of PEL layers on an area smaller than 0.02 μm^2 by the single particle lSPR method. However, in this case the signal noise was substantial larger (around the signal change caused by a single PEL layer). The main reasons for the noise were the lower intensity of the detected scattered light from the single nanoparticle as well as mechanical instability. Further, we used two approaches to yield the thickness and refractive index of the adsorbed layers. We showed that these parameters can be determined either by exploiting the non-linear signal change in lSPR system or by using two different plasmon transducer in lSPR systems,. Although the results were hampered by a certain uncertainty, we suggest using large silver nanoparticles (exhibiting two different plasmon resonances) in lSPR system, which could improve these results.

Conflict of interest

We declare there is no conflict of interest.

Acknowledgment

The project “ImSpec” (FKZ 13N12836), supported by the Federal Ministry of Education and Research (BMBF) Germany, is gratefully acknowledged.

Appendix A. Supplementary data

Supplementary data to this article can be found online at http://dx.doi.org/10.1016/j.sbsr.2016.01.003.

References

[1] J. Popp, M. Strehle, Biophotonics Visions for Better Health Care, Wiley-VCH Verlag GmbH, 2006.
[2] D.K. Kambhampati, W. Knoll, Surface-plasmon optical techniques, Curr. Opin. Colloid Interface Sci. 4 (1999) 273–280.
[3] Anon Reichert Technologies, http://www.reichertspr.com/.
[4] Anon Biacore, https://www.biacore.com.
[5] X.D. Hoa, A.G. Kirk, M. Tabrizian, Towards integrated and sensitive surface plasmon resonance biosensors: a review of recent progress, Biosens. Bioelectron. 23 (2007) 151–160.
[6] J. Homola, S.S. Yee, G. Gauglitz, Surface plasmon resonance sensor: review, Sensors Actuators B Chem. 54 (1999) 3–15.
[7] K.M. Mayer, J.H. Hafner, Localized surface plasmon resonance sensors, Chem. Rev. 111 (2011) 3828–3857.
[8] S. Roh, T. Chung, B. Lee, Overview of the characteristics of micro- and nano-structured surface plasmon resonance sensors, Sensors 11 (2011) 1565–1588.
[9] C. Inhee, C. Yeonho, Plasmonic nanosensors: review and prospect, IEEE J. Sel. Top. Quantum Electron. 18 (2012) 1110–1121.
[10] T. Chung, S.Y. Lee, E.Y. Song, H. Chun, B. Lee, Plasmonic nanostructures for nano-scale bio-sensing, Sensors 11 (2011) 10907–10929.
[11] S. Szunerits, R. Boukherroub, Sensing using localised surface plasmon resonance sensors, Chem. Commun. 48 (2012) 8999–9010.
[12] A.G. Brolo, Plasmonics for future biosensors, Nat. Photonics 6 (2012) 709–713.
[13] W.P. Hall, J.N. Anker, Y. Lin, J. Modica, M. Mrksich, R.P. Van Duyne, A calcium-modulated plasmonic switch, J. Am. Chem. Soc. 130 (2008) 5836–5837.
[14] J. Homola, Surface Plasmon Resonance Based Sensors, Springer, 2006.
[15] C.F. Bohren, D.R. Huffman, Absorption and Scattering of Light by Small Particles, Wiley, New York, 1983.
[16] G. Sun, J.B. Khurgin, Plasmonic enhancement of optical properties by isolated and coupled metal nanoparticles, in: I. Tsukerman, et al., (Eds.) Plasmonics and Plasmonic Metamaterials: Analysis and Applications, vol. 1, World Scientific Publishing Co. Pte. Ltd., ISBN: 9789814355285 2012, pp. 1–44.

[17] L.S. Jung, C.T. Campbell, T.M. Chinowsky, M.N. Mar, S.S. Yee, Quantitative interpretation of the response of surface plasmon resonance sensors to adsorbed films, Langmuir 14 (1998) 5636–5648.
[18] P. Kvasnicka, J. Homola, Optical sensors based on spectroscopy of localized surface plasmons on metallic nanoparticles: sensitivity considerations, Biointerphases 3 (2008) FD4–F11.
[19] J. Voros, The density and refractive index of adsorbing protein layers, Biophys. J. 87 (2004) 553–561.
[20] A.B. Dahlin, J.O. Tegenfeldt, F. Höök, Improving the instrumental resolution of sensors based on localized surface plasmon resonance, Anal. Chem. 78 (2006) 4416–4423.
[21] T. Schneider, N. Jahr, J. Jatschka, A. Csaki, O. Stranik, W. Fritzsche, Localized surface plasmon resonance (LSPR) study of DNA hybridization at single nanoparticle transducers, J. Nanoparticle Res. 15 (2013).
[22] G. Schneider, G. Decher, From functional core/shell nanoparticles prepared via layer-by-layer deposition to empty nanospheres, Nano Lett. 4 (2004) 1833–1839.
[23] S.J. Orfanidis, Electromagnetic Waves and Antennas, www.ece.rutgers.edu/~orfanidi/ewa1999.
[24] P.B. Johnson, R.W. Christy, Optical constants of the noble metals, Phys. Rev. B 6 (1972) 4370–4379.
[25] G. Decher, J.B. Schlenoff, Multilayer Thin Films Sequential Assembly of Nanocomposite Materials, Wiley-VCH Verlag GmbH, 2003.
[26] J.B. Schlenoff, S.T. Dubas, Mechanism of polyelectrolyte multilayer growth: charge overcompensation and distribution, Macromolecules 34 (2001) 592–598.
[27] F.-C. Chien, S.-J. Chen, Direct determination of the refractive index and thickness of a biolayer based on coupled waveguide-surface plasmon resonance mode, Opt. Lett. 31 (2006) 187–189.
[28] P. Adam, J. Dostálek, O. Telezhnikova, J. Homola, SPR Sensor Based on a Bi-diffractive Grating, Proc. SPIE 6585 (2007) 65851Y.
[29] J. Dostalek, P. Adam, P. Kvasnicka, O. Telezhnikova, J. Homola, Spectroscopy of Bragg-scattered surface plasmons for characterization of thin biomolecular films, Opt. Lett. 32 (2007) 2903–2905.
[30] R.I. Nooney, O. Stranik, C. McDonagh, B.D. MacCraith, Optimization of plasmonic enhancement of fluorescence on plastic substrates, Langmuir 24 (2008) 11261–11267.